Scaled Experimental Verification of Single-Well Induction Conductivity Measurement Through Nonmagnetic Casing

Darko Vasić, *Member, IEEE*, Vedran Bilas, *Senior Member, IEEE*, and Anthony J. Peyton

***Abstract*—The electromagnetic induction measurement of dimensions, integrity, or material properties of conductive objects is especially challenging in the case when the electrical conductivity of these objects spans five to seven orders of magnitude. Such an application is the conductivity measurement of the surrounding rocks from within a metal casing of an oil well. The rock conductivity measurement is required in order to determine and revaluate hydrocarbon-bearing layers. We present the first experimental verification of the single-well through-casing induction measurement on a scaled laboratory model of a borehole lined with a stainless steel or copper casing surrounded with a low-conductive medium. The measurements are in the frequency range of 2–16 kHz (10–80 Hz in case of the actual borehole). We explain the theoretical background of the method, describe the scaled model and experimental procedure, and discuss the experimental results. The measurement results are in agreement with the theoretical predictions (relative error less than 15%), and the equivalence of the results for the steel and copper casings (average relative discrepancy less than 10%) corroborates that the rock conductivity measurement can be corrected for variations in the casing properties (dimensions, electrical conductivity, and magnetic permeability).**

***Index Terms*—Cased well, conductivity measurement, eddy currents, electromagnetic induction, rocks, scaled modeling, well logging.**

I. Introduction

ELECTROMAGNETIC induction devices, used for the evaluation of dimensions, integrity, or material properties of conductive objects, are designed for a range of the electrical conductivity across one or two orders of magnitude, e.g., rock conductivity measurement from an open (uncased) borehole (0.1–5 S/m), water level and conductivity measurements (1–15 S/m), monitoring of the graphite core in nuclear reactors (10–100 kS/m) or casing, and tube inspection in oil wells and heat exchangers (1–58 MS/m) [1]–[5]. Particularly challenging are the induction measurements where the properties of both high- and low-conductive objects, with the conductivity spanning five to seven orders of magnitude, must be evaluated. Such an application is the conductivity measurement of the surrounding rocks from within a metal casing of an oil well [6], [7].

The induction rock conductivity measurement from an open (uncased) borehole is a well-logging method routinely used for the evaluation of rock porosity and water saturation, which are essential for the determination of hydrocarbon producibility [8]. In its basic configuration, an induction tool uses a transmitter coil energized at frequencies in the range of 10–100 kHz and a receiver coil to measure the electromagnetic field affected by the rock formation containing water (more conductive) or hydrocarbons (less conductive) [9], [10]. The effect of the rock formation increases with the frequency. However, the dielectric properties of rocks cannot be ignored above 100 kHz, and this complicates the interpretation of the measurement results [8]. Additional receiver coils at different separations from the transmitter improve the receiver array's overall sensitivity, vertical resolution of rock layers' boundaries, and radial investigation depth. Modern multiarray induction tools use a set of coil arrays whose data are combined through inverse problem algorithms in order to further improve the vertical and the radial response [8]. Because of its usefulness in the open-hole environment, it has been recently proposed to apply the induction method inside boreholes lined with a metal casing [6].

An oil-well casing ensures the stability of the well and isolates the well interior from the rock formation. At the location of a hydrocarbon-bearing rock layer, the casing is perforated, enabling the flow of the fluids into the well. The rock conductivity measurement through the casing is required in order to evaluate the remaining potential of the cased well or to locate hydrocarbon-bearing layers that were bypassed during the casing perforation. This is usually the case with the older wells (drilled and cased prior to the modern open-hole tools) or wells that were cased immediately after the drilling due to the hole stability problems. Because of the bypassed layers, the volume of produced (recovered) oil can be as low as 20% of the estimated original oil in place [11]. Using a single-well through-casing rock conductivity measurement, one could avoid drilling a second well for the sole purpose of data gathering.

The theoretical studies of the single-well through-casing induction measurement proposed the coil configuration and excitation frequency range and investigated the sensitivity to the rock conductivity and spatial resolution [6], [7], [12]–[14]. Since any variations in the rock conductivity can be masked

Manuscript received June 22, 2012; revised October 27, 2012; accepted December 13, 2012. Date of publication January 28, 2013; date of current version April 3, 2013. This research was supported in part by the Croatian Ministry of Science, Education and Sport through the research project "Intelligent systems for measurement of difficult-to-measure variables" under Grant 036-0361621-1625 and in part by the Seventh Framework Programme of the European Union through Grant 285939 FP7-REGPOT-2011-1 (ACROSS). The Associate Editor coordinating the review process for this paper was Dr. Jiong Tang.

D. Vasić and V. Bilas are with the Faculty of Electrical Engineering and Computing, University of Zagreb, 10000 Zagreb, Croatia (e-mail: darko.vasic@fer.hr).

A. J. Peyton is with the School of Electrical and Electronic Engineering, University of Manchester, M13 9PL Manchester, U.K.

Digital Object Identifier 10.1109/TIM.2013.2238031

by even minute changes in the casing dimensions and material properties (electrical conductivity and magnetic permeability), a spatial low-pass filtering and measurement of the casing properties have been proposed for the casing effect correction [6], [13], [14].

In this paper, we present the first experimental verification of the through-casing induction measurement on a scaled laboratory model of a metal-cased borehole surrounded with a low-conductive medium (saline solution). The actual oil-well casings are overwhelmingly manufactured from magnetic heat-treated carbon steel, although stainless steel is also used [15], [16]. In this paper, we used copper and stainless steel *American Iron and Steel Institute* (AISI) 304 casings. The AISI 304 steel is slightly magnetic with relative magnetic permeability of 1–10, depending on the material processing. The attenuation of the magnetic field (receiver signal) inside a metal casing increases primarily with the casing factor (i.e., product of the casing wall thickness and the square root of the permeability–conductivity product) [13]. The attenuation in the copper casing is lower than the attenuation of the magnetic steel casing of the same dimensions, whereas it is higher than the attenuation of the nonmagnetic steel casing—copper is a nonmagnetic material but at least ten times more conductive than steel (58 MS/m versus 1–5 MS/m). Thus, the choice of the copper and AISI 304 casings in the scaled model is a good starting point for this first experimental study of the single-well through-casing rock conductivity measurement.

The aim of this paper is to experimentally corroborate two important conclusions made in previous theoretical studies on the single-well through-casing rock conductivity measurement: The phase of the receiver signal is sensitive to the changes of the conductivity of the low-conductive material surrounding the metal casing, and the phase change is independent of the casing dimensions and material properties. The latter opens up the way for the casing effect correction procedure as proposed in [14]. Furthermore, we compare the experimental results with the predictions of an analytical model. This scaled experimental study is a necessary step before designing the full-scale prototype device. This paper contains a substantially extended presentation of the experimental results first published in [17].

This paper is organized as follows. In Section II, we explain the theoretical background of the proposed method, and we briefly describe the analytical model used for the comparison with the experimental results. In Section III, we describe the scaled experimental setup, scaling relations, electronic instrumentation, and experimental procedure. In Section IV, we present and discuss the experimental results. Section V contains the conclusions.

II. Theoretical Background

A. Through-Casing Induction Measurement

A transmitter coil and receiver coils are axially centered inside the cased well and moved along its length to obtain a log of conductivity of rock formation layers and the casing's physical condition. The latter is used in the correction of the casing effect as described in [13], and it is based on the existing casing inspection induction tools [18]. Important design parameters of a through-casing induction device are the locations of the receivers with respect to the transmitter, and the choice of the excitation frequencies.

Inside the metal oil-well casing, the magnetic field of the transmitter coil rapidly decreases with the excitation frequency and the distance from the coil. While the casing has a significant effect on both the magnitude and phase of the receiver signal (induced voltage), the surrounding low-conductive rocks affect only the phase of the receiver signal [6]. Because the attenuation of the receiver signal inside the casing can easily exceed 150 dB, the excitation frequency, proposed in the theoretical studies [1], [6], [12], is below 100 Hz (in comparison to the 10–100-kHz range in the open-hole case). Because of such a low frequency, a larger volume of the low-conductive material is required in order to affect the phase of the receiver signal. Consequently, the transmitter–receiver distance must be increased from around 1 to 5 m [1], [6], [12]. Thus, there is a tradeoff between the sensitivity to the surrounding low-conductive material and the receiver signal attenuation.

Let $\varphi(\sigma_R)$ be the phase of the voltage induced in the receiver inside the casing surrounded by the rocks of conductivity σ_R. Furthermore, let φ_C be the phase of the receiver signal inside the same casing, but with no surrounding rocks. Under the assumption that the current induced in the surrounding low-conductive rocks has no effect on the current distribution within the casing, it can be shown that the phase difference

$$\Delta\varphi(\sigma_R) = \varphi(\sigma_R) - \varphi_C \tag{1}$$

linearly increases with the rock conductivity and excitation frequency [7]. Most importantly, it does not depend on the casing properties [12], [14]. A more detailed explanation of (1) is given in the Appendix. The phase φ_C can be estimated from the measurement of the casing properties using several receiver coils closer to the transmitter coil [13]. Increasing the coil separation and excitation frequency increases the phase sensitivity to the rock conductivity, but it also decreases the signal-to-noise ratio and vertical resolution [12].

B. Analytical Model

We derived the analytical model of the magnetic field distribution of a single-turn transmitter coil axially centered inside a tube made of conductive and permeable material surrounded with cylindrically layered low-conductive medium, as depicted in Fig. 1. In contrast to the usual Dodd–Deeds integral formulation, we truncated the solution region and, as a consequence, formulated the solution of the vector magnetic potential equation as a series [12], [19]. The problem domain should be at least ten times larger than the separation between the transmitter and receiver coils.

The transmitter coil is driven by a sinusoidal current i of constant amplitude I and frequency $\omega = 2\pi f$. The casing has inner radius r_1, outer radius r_2, and wall thickness $c = r_2 - r_1$. The casing material is assumed to be linear, isotropic, and homogeneous with electrical conductivity σ and relative magnetic permeability μ_r. The casing is surrounded with two low-conductive cylindrical layers A and B with conductivity values σ_A and σ_B. This configuration of a layered surrounding

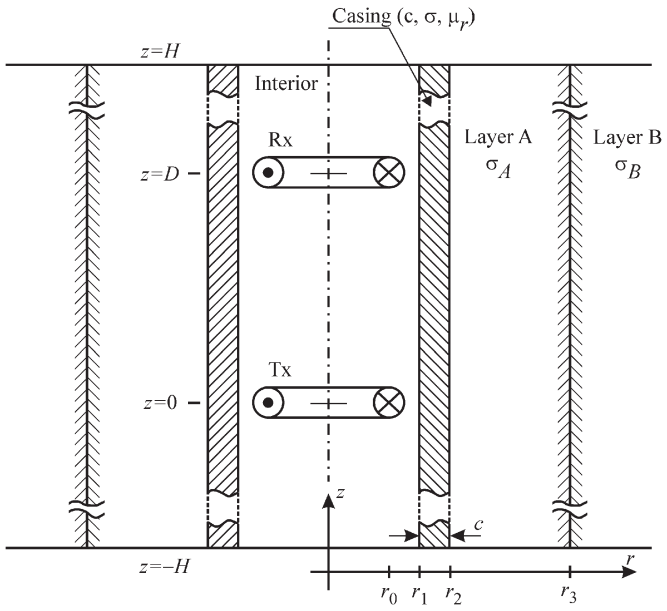

Fig. 1. Geometry used in analytical modeling of the transmitter magnetic field inside the casing surrounded with the cylindrical two-layered low-conductive medium. In the experiments, $\sigma_R = \sigma_A$, and $\sigma_B = 0$.

medium allowed in the previous studies the fundamental theoretical analysis of the coil configurations, choice of excitation frequencies, casing effect, sensitivity to the low-conductive medium, and maximum radius of investigation [12]. Another configuration with horizontally layered medium was used for the analysis of the vertical resolution of a tool [12]. In this paper, we use the configuration with $\sigma_R = \sigma_A$ and $\sigma_B = 0$ for comparison to the experimental results.

Due to the axial symmetry, the vector magnetic potential has the φ-component only, and for the casing interior, it can be represented as the series

$$A(r,z) = \frac{2\mu_0 I}{H} \sum_{i=1}^{N} \cos(\alpha_i z) I_1(\alpha_i r) C_{1,i} \tag{2}$$

where H is the domain's height, which defines the discrete eigenvalues $\alpha_i = \pi(2i-1)/(2H)$, N is a maximum number of the elements in the truncated sum, I_1 is the modified Bessel function of the first kind, and coefficients C_1 are functions of the transmitter, casing properties, and surrounding medium, i.e., $C_{1,i}(\alpha_i, \omega, r_0, r_1, c, \mu_r, \sigma, r_3, \sigma_A, \sigma_B)$. Other symbols are defined in Fig. 1. Coefficients C_1 are obtained solving a set of linear equations that arise from the boundary and interface conditions. The equations are the same as in [20] and [21] if there are no horizontal interfaces. The horizontal interfaces are treated in a similar manner as in [12] or [22]. Voltage induced in a receiver coil coaxially placed at the distance $z = D$ from the transmitter coil is proportional to the product of excitation frequency ω and the transmitter's potential $A(r_0', D)$, where r_0' is the receiver radius, i.e.,

$$U(\omega, D) \propto j\omega 2\pi r_0' A\left(r_0', D\right). \tag{3}$$

The phase of $U(\omega, D)$ will be used in comparison to the experimental results in the following sections.

The model was implemented using MATLAB. It takes about 100 ms to calculate the magnetic field (induced voltage) at the location of the receiver coil using a personal computer with Intel Quad CPU and 4 GB of RAM. More details on the numerical implementation can be found in [13].

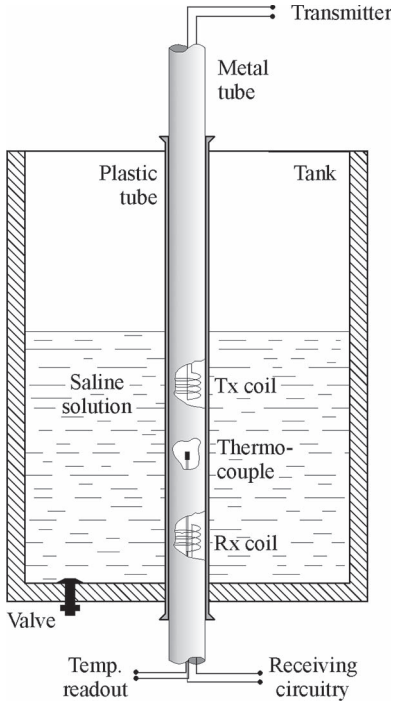

Fig. 2. Schematic representation of the scaled model of the cased borehole.

III. Experimental Setup

A. Scaled Laboratory Model

Physical scale modeling is an important technique for obtaining the electromagnetic response of large systems that would be otherwise impossible to realize in a laboratory [23], [24]. A field system or model is an actual target measurement situation with realistic dimensions. A scaled model has all dimensions scaled, as well as the frequency or time range, the electromagnetic properties of media, and the strength of the electromagnetic field. The coordinates in the field system are related to the coordinates in the scaled model using the length scale factor k_l

$$x = k_l x', \quad y = k_l y', \quad z = k_l z' \tag{4}$$

where primed quantities belong to the scaled model. The fields $\mathbf{E}$, $\mathbf{H}$, and time t or frequency f are scaled as

$$\mathbf{E} = k_e \mathbf{E}', \quad \mathbf{H} = k_h \mathbf{H}', \quad t = k_t t', \quad f = \frac{1}{k_t} f'. \tag{5}$$

Our choice is that all materials in the field and scaled systems have the same electromagnetic properties. Also, we choose that the transmitter currents in the field and scaled systems are equal. As a result of these two choices, the following holds [23]:

$$\begin{aligned} &k_l \text{ is arbitrary,} \\ &k_t = k_l^2, \\ &k_e = \frac{1}{k_t}, \quad k_h = \frac{1}{k_l}. \end{aligned} \tag{6}$$

The laboratory scaled model of a cased borehole is schematically depicted in Fig. 2. The plastic tank can be filled from the

TABLE I
PROPERTIES OF THE SCALED MODEL AND THE FIELD SYSTEM FOR TIME AND LENGTH SCALE FACTORS $k_l^2 = k_t = 200$

Quantity	Scaled model	Field system
Metal tube (casing)		
Outer radius	1.1 cm	15.56 cm
Wall thickness (copper)	0.1 cm	1.414 cm
Wall thickness (AISI 304)	0.15 cm	2.121 cm
Length	2 m	28.3 m
Tank (rock annulus)		
Radius	0.15 m	2.12 m
Height	0.48 m	6.8 m
Coils		
Height	4 cm	56 cm
Mean radius	0.41 cm	5.8 cm
Mean separation	0.34 m	4.8 m
Frequency	2 kHz – 16 kHz	10 Hz – 80 Hz
Electrical conductivity and magnetic permeability	Identical Copper casing: conductivity 58 MS/m, rel. permeability 1 Stainless steel casing: conductivity 1.6 MS/m, rel. permeability ~1 Saline solution: conductivity 15.5 S/m	

top and drained using the valve at the bottom. The transmitter coil, the receiver coil, and a thermocouple are mounted on a plastic rod, inserted into the metal tube, and connected to their respective interfaces; see Section III-B.

The typical production oil-well casing is from 11.4 cm (4 1/2 in) to 24.5 cm (9 5/8 in) in diameter, and its wall thickness is in the range of 0.5–2.3 cm [15], [25]. Using the length scale factor $k_l^2 = 200$, an oil-well casing with the diameter and wall thickness within the specified standard range is modeled by the copper or AISI 304 steel tubes with dimensions as in Table I. The dimensions of the coils and excitation frequency for both systems are also given in Table I.

The material properties are identical in both systems. We used tap water and a saline (NaCl) solution as nonconductive and conductive rocks, respectively. Tap water has conductivity less than 0.05 S/m, and the saline solution has the conductivity of 15.5 S/m. Since the response of an induction device depends on both the volume and conductivity of the surrounding medium, the solution is more conductive than its real-world counterpart (rocks) in order to account for small tank volume [1]. Containers with the solution and tap water were held in the laboratory before the experiments and achieved a stable temperature of $(26.5 \pm 0.5)\ ^\circ$C.

B. Instrumentation

The transmitter coil was driven using an amplifier based on a Texas Instruments (Dallas, US-TX) LM3875T audio power amplifier. The amplifier's input was connected to an Agilent (Santa Clara, US-CA) 33250A function generator. The excitation current (amplitude of 0.75 A) was monitored with a Tektronix (Beaverton, US-OR) TM502A current probe. The temperature of the metal tube was monitored by a Fluke (Everett, US-WA) 80TK thermocouple module connected to a Fluke 45 multimeter. The receiver coil was connected to a differential amplifier (differential gain of 2000, cutoff frequency of 29 kHz, input impedance of 130 MΩ, common-mode rejection ratio around 120 dB below 200 Hz with a 20-dB fall per decade at the gain of 2000 and the input common-mode voltage of 1 V, and equivalent input noise of 4.2 $\text{nV}/\sqrt{\text{Hz}}$), followed by a dual-amplifier bandpass (DABP) filter with easily adjustable resonant frequency between 2 and 20 kHz in discrete steps, bandwidth of 500 Hz, and gain of 2, 30, 60, or 120 [26]. The conductivity of the solution was measured using a Mettler-Toledo (Greifensee, CH) S47 conductivity meter.

The outputs of the current probe, the receiver amplifier, and the multimeter were digitized using a 16-b National Instruments (Austin, US-TX) NI USB-6211 digital acquisition module connected to a battery-powered laptop running a proprietary National Instruments LabVIEW monitoring application. The main task of the monitoring application was a digital phase-sensitive detection (lock-in amplifier) for the measurement of the phase difference between the excitation current signal and the voltage induced in the receiver. The two signals were sampled with 125 kHz each. The low-pass filtering at the last stage of the lock-in amplifier used 2.4 s worth of samples.

C. Experimental Procedure

The experiment for each tube (copper or AISI 304) was conducted in five alternating steps of the empty tank and the tank filled with the saline solution. We denoted these steps as E1, F2, E3, F4, and E5, where E stands for empty tank, F stands for full tank, and the numbers denote the order of the steps. In each step, the amplitude and phase of the receiver signal with respect to the excitation were measured at six frequencies (2.0355, 2.8355, 4.0827, 6.0080, 12.0415, and 15.4100 kHz), which are determined by the DABP filter characteristic. At each frequency and during each step, 100 values of the amplitude and phase were determined from 100 acquired data blocks of length 2.4 s (300 000 samples at 125 kHz). The casing temperature was measured after each data block. The phase difference $\Delta\varphi(\sigma_R)$ of (1) is calculated from the measurements made when the tank is filled with the saline solution and when it is empty.

The temperature of the saline solution varies for $\pm 0.5\ ^\circ$C, but this does not change observably its conductivity (around 2% increase per 1 °C) [27]. However, the casing temperature variations are not negligible. The sources of this change are heating from the transmitter coil when the tank is empty, cooling when the tank is filled with the saline solution, and daily

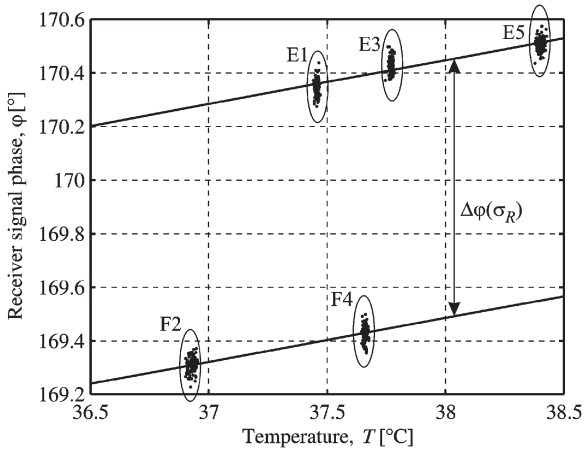

Fig. 3. Measured receiver signal phase at frequency of 12.0415 kHz against the casing temperature for all five steps (each step contains 100 measured values). Full lines are the results of the linear regression using (7). The distance between the lines is temperature-compensated phase difference $\Delta\varphi(\sigma_R)$. E denotes steps with the empty tank. F denotes steps with the tank with saline solution. Numbers denote the order of the steps.

variations of the laboratory temperature. The parameters of the casing (most notably, the casing's conductivity) change with the temperature, and this causes variations in the measured phase.

The casing temperature variations are less than ± 3 °C, and one can assume that the relative variations in the casing parameters are small and linear [28], [29]. According to modeling predictions, the corresponding change of the phase of the receiver signal is also linear. Fig. 3 depicts the measured phase for all steps (100 data points per each step) against the casing temperature for a frequency of 12.0415 kHz. It can be seen that the phase linearly depends on the temperature with the same slope but different offset for E and F steps.

Consequently, the required phase difference $\Delta\varphi(\sigma_R)$ for each frequency was determined in the following way. The phase of the receiver signal is modeled as

$$\varphi = bT + \Delta\varphi(\sigma_R)h + \varphi_0 \tag{7}$$

where φ is the measured phase of the receiver signal, b is the slope, T is the casing temperature, h is a binary variable equal to 1 if the observation comes from F steps and 0 if it comes from E steps, and φ_0 is the offset caused by the casing effect and the measurement chain frequency characteristic. A total of 500 measured phase values from all five steps (three with the empty tank and two with the full tank) are grouped as observations (φ_i, T_i, h_i) and parameters b, $\Delta\varphi(\sigma_R)$ and φ_0 are determined using linear regression. As a result, two parallel least squares lines are obtained as depicted in Fig. 3. Uncertainties in parameters $(b, \Delta\varphi(\sigma_R), \varphi_0)$ can be calculated from the covariance matrix and the estimate of the standard deviation of observations φ_i [30].

The similar procedure holds for the temperature compensation of the receiver signal amplitude with the temperature model as

$$U = mT + U_0 \tag{8}$$

where m is the slope and U_0 is the initial offset. There is no h-related parameter since the receiver signal amplitude is not sensitive to the surrounding low-conductive medium.

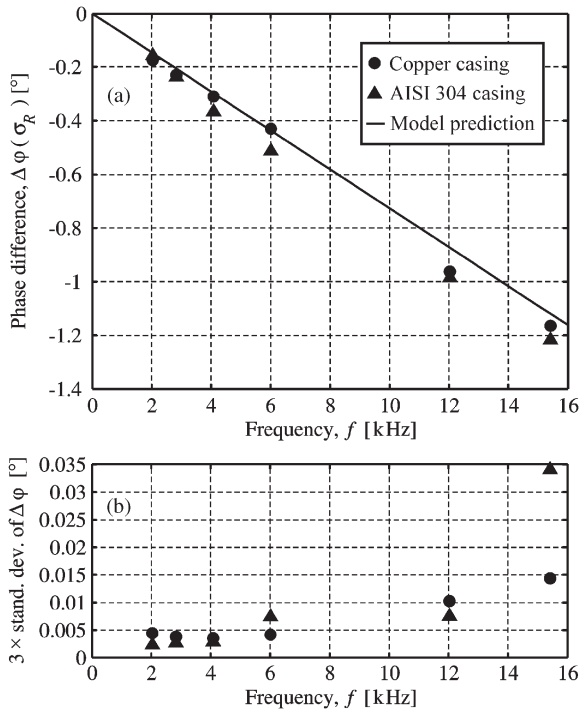

Fig. 4. (a) Frequency dependence of measured phase difference $\Delta\varphi(\sigma_R)$ as defined in Fig. 3 for copper and AISI 304 casings. The full line is a result of the model from Section II-B. (b) Uncertainty of the phase difference estimated from the linear regression and given as triple value of the standard deviation.

IV. Results and Discussion

In a preliminary study [17], we showed that there were no detectable differences in the amplitude and phase of the receiver signal when the tank was empty and full of tap water, whereas in the case of the tank filled with the saline solution, the amplitude remained unchanged, but the phase changed. The conclusion that this change is due to the inductive coupling with the surrounding medium, and not due to the capacitive coupling, was corroborated by the insensitivity to the negligibly conductive tap water and by the good agreement of the experimental results with the theoretical predictions. We omit the details of these results in this paper for the sake of shortness and clarity and because they are a subset (copper tube and excitation frequency of 12.0415 kHz) of the results reported here.

The phase difference $\Delta\varphi(\sigma_R)$ measured, as described in Section III-C, for six values of the excitation frequency is shown in Fig. 4(a) for copper and AISI 304 casings. Also, the model prediction is depicted using dimensions of the scaled setup and the surrounding medium conductivity of 15.5 S/m. The modeling results are the same regardless of the casing material [thus, only one line in Fig. 4(a)]. Based on the results, one can make two important observations. First, the data measured with copper and AISI 304 casings and the modeled data are in a good agreement (with relative error less than 15%), confirming the inductive character of the coupling between the coils and the surrounding medium. Second, the measured phase differences for copper and stainless steel casings are quantitatively comparable as suggested by the model. Average relative discrepancy between the phase differences measured for the copper and steel casings is less than 10% across the frequency range. Since the

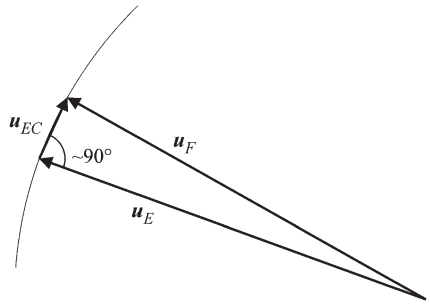

Fig. 5. Superposition of primary receiver signal (empty tank) $\boldsymbol{u}_E$ and eddy current component from the low-conductive medium $\boldsymbol{u}_{EC}$. The result is the total receiver signal $\boldsymbol{u}_F = \boldsymbol{u}_{EC} + \boldsymbol{u}_E$.

casings are on the opposite sides of the expected conductivity interval, the second observation corroborates that the phase change is independent of the casing and confirms the feasibility of the casing effect correction procedure as stated in (1). The increase of the measured phase difference with the frequency indicates that one should choose the highest possible frequency for the measurement of the rock conductivity. The upper limit is the attenuation of the casing that degrades the signal-to-noise ratio beyond the acceptable level. The triple value of the standard deviation (99.7% confidence interval) for each measurement point from Fig. 4(a) is shown in Fig. 4(b). The triple relative measurement uncertainty of the phase difference is less than 3.5%.

As explained in the Appendix, the total receiver signal $\boldsymbol{u}_F$ (full tank), which is proportional to the magnetic field, is connected to the primary receiver signal (empty tank) $\boldsymbol{u}_E$ via the formation factor k_R

$$\boldsymbol{u}_F = k_R \boldsymbol{u}_E = \boldsymbol{u}_E + (k_R - 1)\boldsymbol{u}_E = \boldsymbol{u}_E + \boldsymbol{u}_{EC} \qquad (9)$$

where component $\boldsymbol{u}_{EC}$ is due to the eddy currents induced in the low-conductive saline solution. The formation factor is $k_R \approx 1 - j(z/\delta)^2$ for the ratio of the transmitter–receiver distance to the penetration depth of the eddy currents $z/\delta \ll 1$; see the Appendix. In this case and according to (9), component $\boldsymbol{u}_{EC}$ of the total (full tank) receiver signal $\boldsymbol{u}_F = \boldsymbol{u}_E + \boldsymbol{u}_{EC}$ lags the primary (empty tank) receiver signal $\boldsymbol{u}_E$ by approximately 90°, whereas $\boldsymbol{u}_F$ and $\boldsymbol{u}_E$ have approximately the same magnitudes, as illustrated in Fig. 5 [31]. One can observe this too in the measurement results. The difference in the receiver signal amplitude U between E and F steps for all measurements is less than 2.2‰ relative to the amplitude in the E steps (see Fig. 6). The lag $\angle \boldsymbol{u}_{EC}$, shown in Fig. 7 and calculated using (9) from the mean amplitude and phase of the receiver signal in E and F steps, is between 90.1° and 90.6°, assuming temperature correction as in (7) and (8). The lag in Fig. 7 increases with the frequency due to the effect of neglected higher order terms in the series expansion of k_R; see the Appendix.

V. Conclusion

We presented the first experimental verification of the through-casing induction measurement on a scaled laboratory model of a borehole lined with nonmagnetic metal (copper and stainless steel) casing surrounded with the low-conductive medium. The experiment confirmed that it is possible, using common electronic instrumentation, to observe the presence of the low-conductive medium through a highly conductive metal tube by measuring the phase of the receiver coil signal. The measurement results are in agreement with the theoretical predictions. The measured effect is from the inductive coupling with the low-conductive medium. The validity of the casing effect correction procedure is confirmed since the results are the same for the copper and stainless steel casings. Further steps include experiments with ferromagnetic steel tubes and variation of the conductivity of the surrounding medium, in order to determine the measurement resolution and sensitivity.

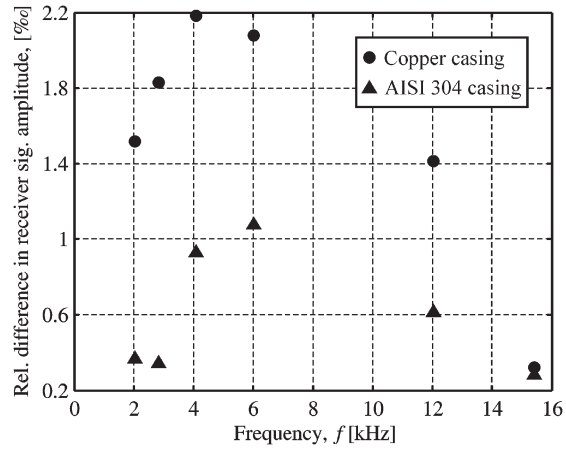

Fig. 6. Difference in the receiver signal amplitude U between E and F steps relative to the amplitude in the E steps.

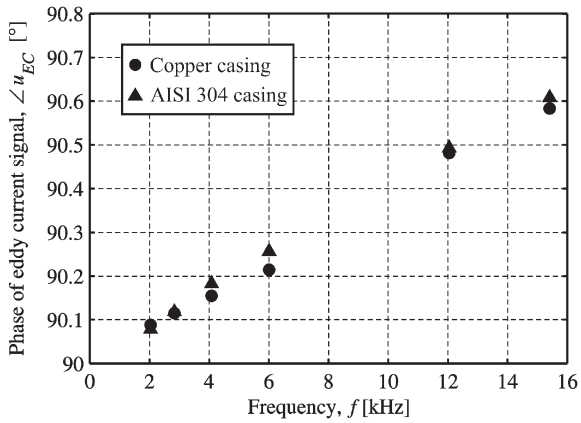

Fig. 7. Frequency dependence of the lag of component $\boldsymbol{u}_{EC}$, induced by the eddy currents in the saline solution, relative to the primary receiver signal $\boldsymbol{u}_E$ (with empty tank). The increase with the frequency is due to the higher order terms in the expansion of (14).

Appendix

At a large distance from the transmitter (ten transmitters' radii), its vector potential can be approximated with the potential due to a magnetic dipole of moment

$$m = I\pi r_0^2. \qquad (10)$$

For $z \gg r_0$, the axial component of the magnetic field magnitude of the transmitter in air along the z-axis is

$$B_{z,air}(r=0,z) = \mu_0 \frac{m}{2\pi z^3}. \quad (11)$$

If the transmitter is positioned inside the casing, the magnetic field at distances $z \gg r_0$ will be severely attenuated, but its magnitude will still be proportional to $r_0^2 z^{-3}$. Because of that proportionality, the magnetic field $B_{z,C}$ of the dipole inside the casing with moment m_C can be related to the dipole in the air with moment m and magnetic field $B_{z,air}$

$$B_{z,C}(r=0,z) = \mu_0 \frac{m_C}{2\pi z^3} = \mu_0 \frac{k_C m}{2\pi z^3} = k_C B_{z,air}(r=0,z) \quad (12)$$

where complex function k_C is a casing attenuation factor, which depends on the casing properties and excitation frequency. Numerical simulations in [12] and [14] reveal that the magnitude of k_C does not depend on z for $z \gg r_0$. This confirms the dipole character (i.e., the cubic dependence on z) of $B_{z,C}$.

If a magnetic dipole is placed in the homogeneous conductive medium (rocks) without the casing, the magnetic field along the z-axis also shows $r_0^2 z^{-3}$ dependence. Similarly to the previous situation with the casing alone, we can write for an effective moment of the dipole in this case $m_R = k_R m$. The rock formation factor k_R depends on the rock conductivity and excitation frequency. A simple closed-form solution can be found for $z \gg r_0$ [9], [32]

$$B_{z,R}(r=0,z) = \mu_0 \frac{m_R}{2\pi z^3} = \mu_0 \frac{k_R m}{2\pi z^3} = k_R B_{z,air}(r=0,z). \quad (13)$$

If the penetration depth is $\delta = \sqrt{2/(\omega \mu_0 \sigma_R)}$, the formation factor k_R is

$$k_R = \left(1 + \frac{z}{\delta} + j\frac{z}{\delta}\right) \exp\left(-\frac{z}{\delta} - j\frac{z}{\delta}\right). \quad (14)$$

If the penetration depth is much larger than the transmitter–receiver distance and using the series expansion of (14) around $z/\delta = 0$, k_R can be approximated with

$$k_R \approx 1 - j\frac{z^2}{\delta^2}. \quad (15)$$

If we assume that the surrounding medium changes the far field of a dipole inside the casing in the same way as it changes the field of the dipole without the casing, we can write the magnetic field in the presence of the casing and the rocks as

$$B_{z,C+R} = k_R B_{z,C} = k_R k_C B_{z,air}. \quad (16)$$

This can be justified by the dipole nature of the magnetic field of the transmitter inside the casing and by the fact that the induced current flowing in the medium has no effect on the current distribution within the casing. The same conclusions were corroborated by numerical and scaled experimental studies for other configurations, e.g., surface-to-borehole measurements in [14].

The importance of (16) is in a simple correction of the rock conductivity measurement for variations in the casing properties. The casing attenuation can be calculated and compensated if one measures the casing properties [13]. In other words, the casing acts as a low-pass filter for which the inverse of its transfer function can be calculated for known casing properties. From (16), it follows that

$$B_{z,C+R} = |k_R||k_C| B_{z,air} \exp\left(j(\arg k_R + \arg k_C)\right) \quad (17)$$

where $B_{z,air}$ is real valued. If it is possible to calculate $B_{z,C}$ from the measured casing properties, then

$$\Delta\varphi(\sigma_R) = \arg B_{z,C+R} - \arg B_{z,C} = \arg k_R \quad (18)$$

which corresponds to (1). The simulations of the real-size case for a fixed σ_R showed the maximal deviation of only 0.005° between the open-hole value arg $B_{z,R}$ and values of $\Delta\varphi(\sigma_R)$ for the casing properties in the ranges of 1–10 MS/m for the conductivity, 1–200 for the relative permeability, and 2–20 mm for the wall thickness [7], [12]. These ranges are larger than the expected ranges of the actual casings.

ACKNOWLEDGMENT

D. Vasić would like to thank the British Scholarship Trust for the support during his stay at the University of Manchester. The authors would also like to thank M. Kuri and Ž. Lučev Vasić for their help with the experimental setup.

REFERENCES

[1] A. A. Kaufman and Y. A. Dashevsky, *Principles of Induction Logging*. Amsterdam, The Netherlands: Elsevier, 2003, ser. Methods in Geochemistry and Geophysics, 1st ed.

[2] W. Yin, A. J. Peyton, G. Zysko, and R. Denno, "Simultaneous noncontact measurement of water level and conductivity," *IEEE Trans. Instrum. Meas.*, vol. 57, no. 11, pp. 2665–2669, Nov. 2008.

[3] D. Vasić, V. Bilas, and D. Ambruš, "Pulsed eddy-current nondestructive testing of ferromagnetic tubes," *IEEE Trans. Instrum. Meas.*, vol. 53, no. 4, pp. 1289–1294, Aug. 2004.

[4] B. Dekdouk, C. Ktistis, D. W. Armitage, A. J. Peyton, R. Chapman, and M. Brown, "Non-contact characterisation of conductivity gradient in isotropic polycrystalline graphite using inductance spectroscopy measurements," *Insight-Non-Destruct. Test. Condition Monit.*, vol. 53, no. 2, pp. 90–95, Feb. 2011.

[5] J. Íñiguez, V. Raposo, and P. Hernández, "Contactless technique for low-frequency measurement of resistivity in nonmagnetic conductive tubes," *IEEE Trans. Instrum. Meas.*, vol. 56, no. 2, pp. 418–421, Apr. 2007.

[6] H. J. Kim and K. H. Lee, "Electromagnetic fields in a non-uniform steel-cased borehole," *Geophys. Prospect.*, vol. 54, no. 4, pp. 433–439, Jul. 2006.

[7] D. Vasić, V. Bilas, and T. Devčić, "On feasibility of inductive conductivity measurement of formation surrounding a metal casing," in *Proc. IEEE IMTC*, Victoria, BC, Canada, May 2008, pp. 186–189.

[8] D. S. Ellis and J. M. Singer, *Well Logging for Earth Scientists*, 2nd ed. Dordrecht, The Netherlands: Springer-Verlag, 2007.

[9] J. H. Moran and K. S. Kunz, "Basic theory of induction logging and application to study of two-coil sondes," *Geophysics*, vol. 27, no. 6, pp. 829–858, Dec. 1962.

[10] R. L. Kleinberg, W. C. Chew, and D. D. Griffin, "Noncontacting electrical conductivity sensor for remote, hostile environment," *IEEE Trans. Instrum. Meas.*, vol. 38, no. 1, pp. 22–26, Feb. 1989.

[11] M. A. Gutierrez, J. Dvorkin, and A. Nur, "Theoretical rock physics for bypassed oil detection behind the casing: La Cira-Infantas oil field," *Lead. Edge*, vol. 20, no. 2, pp. 192–197, Feb. 2001.

[12] D. Vasić, "Measurement of rock resistivity using inductive method in a cased well," Ph.D. dissertation, Fac. Elect. Eng. Comput., Univ. Zagreb, Zagreb, Croatia, 2010.

[13] D. Vasić and V. Bilas, "Application of stochastic inversion to casing effect correction in through casing induction logging," *IEEE Trans. Instrum. Meas.*, vol. 61, no. 5, pp. 1458–1465, May 2012.

[14] A. M. Augustin, W. D. Kennedy, H. F. Morrison, and K. H. Lee, "A theoretical study of surface-to-borehole electromagnetic logging in cased holes," *Geophysics*, vol. 54, no. 1, pp. 90–99, Jan. 1989.
[15] S. S. Rahman and G. V. Chilingarian, *Casing Design—Theory and Practice*, vol. 42. Amsterdam, The Netherlands: Elsevier, 1995, ser. Developments in Petroleum Science.
[16] *Schlumberger Oilfield Glossary*, Sclumberger Ltd., Houston, TX, Jun. 2012. [Online]. Available: www.glossary.oilfield.slb.com
[17] D. Vasić, V. Bilas, and A. J. Peyton, "Induction conductivity measurement of surrounding low-conductive medium from copper tube—Experimental verification," in *Proc. IEEE I2MTC*, Graz, Austria, May 2012, pp. 314–317.
[18] *METT, Multifrequency Electromagnetic Thickness Tool. Datasheet*, Sclumberger Ltd., Houston, TX, Jun. 2012. [Online]. Available: www.slb.com
[19] T. P. Theodoulidis and J. R. Bowler, "The truncated region eigenfunction expansion method for the solution of boundary value problems in eddy current nondestructive evaluation," *Proc. AIP Conf.*, vol. 760, no. 1, pp. 403–408, Apr. 2005.
[20] C. V. Dodd, C. C. Cheng, and W. E. Deeds, "Induction coils coaxial with an arbitrary number of cylindrical conductors," *J. Appl. Phys.*, vol. 45, no. 2, pp. 638–647, Feb. 1974.
[21] D. Vasić, V. Bilas, and B. Šnajder, "Analytical modelling in low-frequency electromagnetic measurements of steel casing properties," *NDT&E Int.*, vol. 40, no. 2, pp. 103–111, Mar. 2007.
[22] H. Sun, J. R. Bowler, and T. P. Theodoulidis, "Eddy currents induced in a finite length layered rod by a coaxial coil," *IEEE Trans. Magn.*, vol. 41, no. 9, pp. 2455–2461, Sep. 2005.
[23] F. C. Frischknecht, "Electromagnetic physical scale modeling," *Electromagn. Methods Appl. Geophys.*, vol. 1, pp. 365–441, 1988.
[24] F. Gao and D. P. Shattuck, "A scale model of the through-casing resistivity measurement," in *Proc. 4th ICSP*, 1998, vol. 2, pp. 1589–1592.
[25] *Specification for Casing and Tubing*, Std. ISO 11960:2004/API 5CT, 8. ed.
[26] A. B. Williams and F. J. Taylor, *Electronic Filter Design Handbook*, 4th ed. New York: McGraw-Hill, 2006.
[27] M. Hayashi, "Temperature-electrical conductivity relation of water for environmental monitoring and geophysical data inversion," *Environ. Monit. Assess.*, vol. 96, no. 1–3, pp. 119–128, Aug./Sep. 2004.
[28] M. I. Epov, G. M. Morozova, E. Y. Antonov, and I. G. Kuzin, "Method of nondestructive testing for technical state of casing strings in oil and gas wells basing on the transient electromagnetic method," *J. Mining Sci.*, vol. 39, no. 3, pp. 216–224, May 2003.
[29] R. M. Bozorth, *Ferromagnetism*, 7th ed. Princeton, NJ: Van Nostrand, 1963.
[30] P. R. Bevington and D. K. Robinson, *Data Reduction and Error Analysis for the Physical Sciences*, 3rd ed. New York: McGraw-Hill, 2003.
[31] S. Watson, R. J. Williams, W. Gough, and H. Griffiths, "A magnetic induction tomography system for samples with conductivities below 10 S/m," *Meas. Sci. Technol.*, vol. 19, no. 4, pp. 045501-1–045501-11, Apr. 2008.
[32] Y. Song and K. H. Lee, "Electromagnetic fields due to a loop current in a cased borehole surrounded by uniform whole space," Earnest Orlando Lawrence Berkeley Nat. Lab., Berkeley, CA, Tech. Rep. LBNL-42371, Jan. 1998.

Darko Vasić (S'03–M'10) received the Dipl.Ing., M.Sc., and Ph.D. degrees in electrical engineering from the University of Zagreb, Zagreb, Croatia, in 2002, 2005, and 2010, respectively.

He is currently a Postdoctoral Researcher with the Department of Electronic Systems and Information Processing, Faculty of Electrical Engineering and Computing, University of Zagreb. His research interests are in the field of electronic instrumentation and signal processing, specifically electromagnetic measurement methods, networked sensors, signal detection, and inverse problems.

Vedran Bilas (M'98–SM'10) received the Dipl.Ing., M.Sc., and Ph.D. degrees in electrical engineering from the University of Zagreb, Zagreb, Croatia, in 1991, 1995, and 1999, respectively.

He is currently a Professor of electrical engineering with the Department of Electronic Systems and Information Processing, Faculty of Electrical Engineering and Computing, University of Zagreb. He has over 20 years of research and development experience in the area of sensors and electronic systems. His research interests are in the field of electronic instrumentation, intelligent and networked sensors, applied electromagnetism, and signal processing. His recent projects and publications are in the induction methods, design of harsh environment electronic systems, intelligent sensors and interfaces, and wireless sensor networks.

Dr. Bilas was the founder and the Chair of the Croatian Chapter of the IEEE Instrumentation and Measurement Society from 2005 to 2010.

Anthony J. Peyton received the B.Sc. degree in electrical engineering and electronics and the Ph.D. degree with a thesis on "Device for the assessment and rehabilitation of kinetic muscle function and circuitry for monitoring localized muscle fatigue" from the University of Manchester Institute of Science and Technology (UMIST), Manchester, U.K., in 1983 and 1986, respectively.

He was appointed as the Principal Engineer at Kratos Analytical Ltd., Manchester, in 1989, developing precision electronic instrumentation systems for magnetic sector and quadrupole mass spectrometers, from which an interest in electromagnetic instrumentation developed. He returned to UMIST as a Lecturer and worked with the Process Tomography Group. He moved to Lancaster University, Lancaster, U.K., in 1996, taking up the post of Senior Lecturer. He was promoted to Reader in Electronic Instrumentation in July 2001 and Professor in May 2004. Since December 2004, he has been a Professor of Electromagnetic Tomography Engineering with the University of Manchester, Manchester. His main research interests currently are in the area of instrumentation, applied sensor systems, and electromagnetics.